Article

Energy Minimization in Reconfigurable Intelligent Surface-Assisted Unmanned Aerial Vehicle-Enabled Wireless Powered Mobile Edge Computing Systems with Rate-Splitting Multiple Access

Jihyung Kim [1], **Eunhye Hong [2]**, **Jaemin Jung [3]**, **Jinkyu Kang [3]** and **Seongah Jeong [2],***

1   Spatial Wireless Transmission Research Section, Electronics and Telecommunications Research Institute, Daejeon 34129, Republic of Korea; savant21@etri.re.kr
2   School of Electronics Engineering, Kyungpook National University, Daegu 41566, Republic of Korea; ghddms21@knu.ac.kr
3   Department of Information and Communication Engineering, Myongji University, Seoul 17058, Republic of Korea; jjm91548971@mju.ac.kr (J.J.); jkkang@mju.ac.kr (J.K.)
*   Correspondence: seongah@knu.ac.kr; Tel.: +82-53-950-5538

Abstract: In this study, a reconfigurable intelligent surface (RIS)-assisted wireless-powered mobile edge computing (WP-MEC) system is proposed, where a single-antenna unmanned aerial vehicle (UAV)-mounted cloudlet provides offloading opportunities to K user equipments (UEs) with a single antenna, and the K UEs can harvest the energy from the broadcast radio-frequency signals of the UAV. In addition, rate-splitting multiple access is used to provide offloading opportunities to multiple UEs for effective power control and high spectral efficiency. The aim of this paper is to minimize the total energy consumption by jointly optimizing the resource allocation in terms of time, power, computing frequency, and task load, along with the UAV trajectory and RIS phase-shift matrix. Since coupling issues between optimization variable designs are caused, however, an alternating optimization-based algorithm is developed. The performance of the proposed algorithm is verified via simulations and compared with the benchmark schemes of partial optimizations of resource allocation, path planning, and RIS phase design. The proposed algorithm exhibits high performance in WP-MEC systems with insufficient resources, e.g., achieving up to 40% energy reduction for a UAV with eight elements of RIS.

Keywords: mobile edge computing; wireless energy transfer; reconfigurable intelligent surfaces; offloading; unmanned aerial vehicle; rate-splitting multiple access

1. Introduction

The advancement of 6G network technologies has generated low-latency and high-throughput Internet of Things (IoT) applications such as autonomous driving, X-reality (XR), and remote surgery. However, small IoT devices with battery power constraints cannot process large amounts of data required for seamless communication and real-time data computation, which is crucial for such emerging applications. To address this issue, mobile edge computing (MEC) is a promising solution for IoT devices because it provides the computing ability of the edge server, thereby reducing their energy consumption and extending their lifetime [1–3]. Moreover, from radio-frequency signals broadcast nearby the user equipment (UE) of the MEC systems, the energy can be harvested at the battery-power-constrained UE. This is motivated by wireless-powered communication networks (WPCNs) and simultaneous wireless information and power transfer (SWIPT) techniques, and it is referred to as a wireless-powered MEC (WP-MEC) system [4–7]. In this system, it is a key challenge to guarantee the wireless link quality between the UE and edge for reducing

the energy consumption of the UE during offloading and for harvesting the energy for sustaining their operation.

Unmanned aerial vehicles (UAVs), e.g., drones, have been used as an edge server for MEC systems, as the line-of-sight (LOS) link can be easily obtained by adjusting the flying path via their free mobility in a three-dimensional (3D) space [8–10]. In particular, UAV-mounted cloudlets can be deployed in the proximity of the desired offloading devices, obtaining high-quality links, which accelerate to replenish the battery of the UE and transmit the offloaded input and output in WP-MEC systems. However, when severe channel attenuation or physical blockages, such as high-rise buildings and skyscrapers, interfere with the LOS links between the UAV and UE, the performance of such systems deteriorates. In such cases, reconfigurable intelligent surfaces (RISs) can be alternatively used in various communication systems, such as millimeter wave [11], nonorthogonal multiple access (NOMA) [12], and free-space optical (FSO) [13]. By controlling the large number of low-cost reflecting elements of RISs in the vicinity of a transmitter or a receiver, virtual links can be obtained to encourage the preferred signal propagation environment. To this end, we aim at minimizing the energy consumption of WP-MEC systems by leveraging RISs and UAVs.

Main Contributions

Herein, a novel framework of an RIS-assisted WP-MEC system with a UAV-mounted cloudlet is proposed, which uses rate-splitting multiple access (RSMA) for offloading multiple UEs. Under this framework, the resource allocation is jointly optimized in terms of time, power, computing frequencies, and task load, along with the UAV's trajectory and the phase-shift matrix of the RIS. To the best of our knowledge, RSMA-based WP-MEC systems that use UAVs or RISs are at their beginning stage of development, providing insights and roadmaps for future intelligent drone communications. The detailed contributions of this work are as follows:

- In order to effectively reduce the energy consumption of WP-MEC channels, we consider a UAV-mounted cloudlet for obtaining the desired channel links by freely and simultaneously moving the RIS between the UAV and the UE deployed for obtaining additional virtual links. In this system, the problem of minimizing the total energy consumption is formulated over jointly optimizing the resource allocation in terms of time, power, computing frequency, and task load, along with the UAV trajectory and RIS phase-shift matrix. However, the coupling issues between optimization variable designs make it challenging to find a globally optimal solution for the formulated minimization problem. Therefore, an alternating optimization (AO)-based algorithm is developed to converge a locally optimal solution, and its convergence and computational complexity are analyzed.
- For wireless energy transfer (WET) and MEC, a new frame structure with four phases is developed using the harvest-then-computing approach [4], such as the WET phase and offloading phase—the latter comprising three phases for local computing and uploading, computing at the UAV, and downloading the computing results.
- The superiority of the proposed WP-MEC system and algorithm is verified via simulation and numerical analysis. Results reveal that the proposed algorithm can reduce the energy consumption to approximately half of that of the benchmark schemes, which is essential for systems with insufficient resources, such as short mission times or a small number of RIS elements. To the best of our knowledge, the consideration of both RISs and UAV-mounted cloudlets for WP-MEC systems is at its beginning stage of development, and their performances are further improved by using the RSMA technique.

The remainder of this paper is organized as follows. Section 2 describes the system model. Section 3 presents the problem formulation and the proposed algorithm for energy-efficient RIS-assisted WP-MEC systems using the UAV-mounted cloudlet. Section 4 discusses the numerical analysis results, and Section 5 concludes the paper.

2. System Model

Herein, the current state-of-the-art WP-MEC systems are discussed, and the set-up of the proposed model is discussed.

2.1. Related Works

Section 2.1.1 discusses related studies on UV-assisted WP-MEC systems that provide computing and energy resources. Section 2.1.2 discusses the existing studies on RIS-assisted WP-MEC systems used to improve network coverage.

2.1.1. UAV-Assisted WP-MEC Systems

A few recent research works on UAV-assisted WP-MEC systems have begun to be conducted, where the UAV is equipped with energy and computing resources in 3D space. A UAV-enabled WP-MEC system was proposed where the MEC server was implemented on the UAV and the energy signals were used to charge the ground users's batteries [14]. Resource allocation was investigated under the partial computation offloading mode to maximize the weighted sum computation bits by jointly optimizing the transmit power, computing frequencies, time, and UAV trajectory [14]. UAVs with an energy transmitter and a computing server were introduced into WP-MEC systems, wherein the sensor devices executed tasks using the UAV [15]. The problem formulation was also developed to minimize the energy consumption of the UAV by jointly optimizing the offloading amount, CPU frequencies, transmit power, and UAV trajectory. The WP-MEC system was previously designed to minimize the total energy consumption of the UAV that provided the users with energy supply and computation offloading by optimizing the UAV trajectory [16]. UAV-assisted WP-MEC systems can improve the computation capability of UE, thereby enhancing the energy and task offloading efficiencies.

2.1.2. RIS-Assisted WP-MEC Systems

RISs can assist throughput maximization in wireless communication, and their use in WP-MEC systems has been researched. Channel modeling and RIS reflection coefficient designs for various WP-MEC applications have been investigated. An orthogonal frequency division multiplexing-based WP-MEC system comprising multiple single-antenna users and a single-antenna hybrid access point (HAP) was proposed [4], where the RIS was used to reduce the energy consumption of the system. Using the harvest-then-computing protocol, the HAP broadcast the energy signal in downlink for WET and received the offloaded task in uplink for computing. An RIS/UAV-based MEC system was also proposed, wherein one RIS was deployed near the users and the other RIS was deployed around the power beacon [6]. The total flying time of the UAV was minimized using the proposed AO-based method to jointly optimize the RIS phase shifts, flying path, and resource allocation and scheduling. Inspired by these research contributions, the advantages of RIS and UAV in WP-MEC systems are exploited herein.

2.2. Set-Up

Figure 1 shows an RIS-assisted WP-MEC system with RSMA comprising a single-antenna UAV-mounted cloudlet, an RIS attached to a high building surface, and K single-antenna UE. Each piece of UE has a computational task to be processed within the mission time T. All system entities are assumed to be synchronized. This assumption is justified by correlating preambles regularly, as in the existing cellular system, or by periodically handshaking and computing the time offsets and the round-trip delays, as in the existing network time protocols [17] (The robust design against the time offset or imperfect channel state information in asynchronous environments can be easily extended, e.g., by adopting the norm-bounded uncertainty model [18] in the proposed design). To complete task processing, the UE computes a portion of the task locally and offloads the remaining task to the UAV-mounted cloudlet. For these operations, the UE is assumed to be equipped with rechargeable batteries, and the energy from radio-frequency signals broadcast by the

UAV is harvested. Here, RIS with M elements is installed to support energy harvesting and offloading by generating an additional virtual link between the UE and the UAV. Moreover, the RSMA method is applied in the uplink for the efficient multiple access of UE to transmit the offloaded data. For tractability, the total task completion time, T seconds (s), is divided into N equal time slots, each of which has a duration of $\tau = T/N$ in order to be small enough. In other words, the UAV's location can be regarded as remaining relatively stable for each time slot. Each time slot is denoted by $n \in \mathcal{N} = \{1, ..., N\}$.
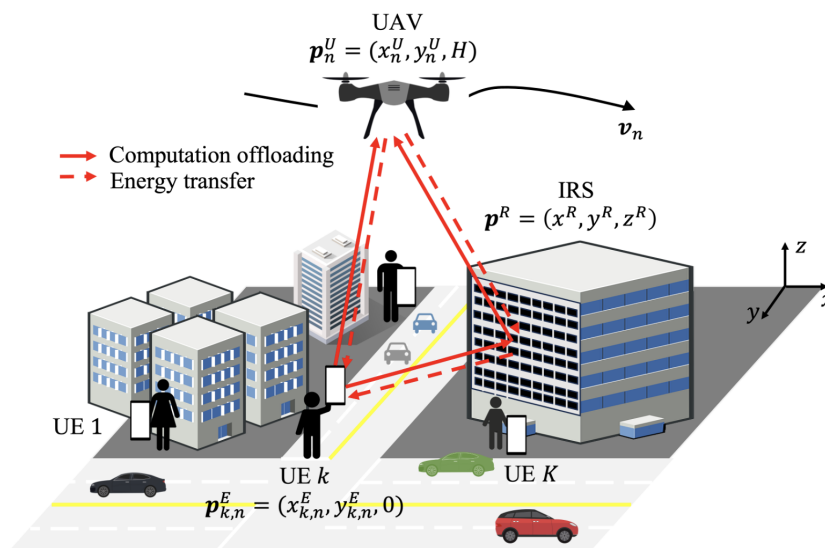

Figure 1. An RIS-assisted UAV-enabled WP-MEC system using RSMA.

To this end, each frame of the system is divided into four phases, illustrated in Figure 2, using the harvest-then-computing technique [5]: (i) WET phase, (ii) local computing and offloading (LO) phase, (iii) UAV's computing phase, and (iv) the downloading phase of the computation results. Specifically, in the WET phase, the UAVs broadcast energy signals to all the UEs to recharge their batteries. Then, in the LO phase, the UE computes the partial task via local computing and transmits the remaining offloaded tasks to the UAV via the uplink RSMA. After receiving the offloaded tasks, the UAV computes them in the computing phase and transmits the computation results via the downlink in the downloading phase. The detailed operations and related signal models for each phase are discussed in the following sections. As the UAV has high-performance processors and higher transmit power than the UE, and the computation results are typically modest in size, the time required for the computing and downloading phases of the UAV can be negligible [5]. Thus, the durations of the WET and LO phases are $\mu_n \tau$ and $(1 - \mu_n)\tau$, respectively, where $0 \leq \mu_n \leq 1$.
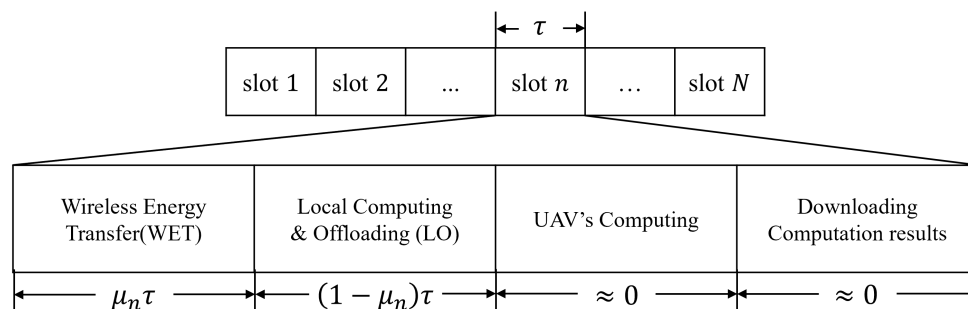

Figure 2. Time structure for the RIS-assisted UAV-enabled WP-MEC system.

The positions of all nodes of the system are modeled using a 3D coordinate system. The UEs are located at $p_k^E = \left(x_k^E, y_k^E, 0 \right)$ in the ground, and the UAV flies at a fixed height of

H (m) at $p_n^U = (x_n^U, y_n^U, H)$ for each time slot n. The starting and final positions of the UAV are $p_1^U = p_I^U$ and $p_N^U = p_F^U$, respectively. To ensure that the UAV has a feasible trajectory, the maximum speed of the UAV is set to V_{max} (m/s), where

$$v_n = \frac{1}{\tau}\left\| p_n^U - p_{n-1}^U \right\| \leq V_{max}, \quad \forall n \in \mathcal{N} - \{1\}. \tag{1}$$

Based on a previous study [7], the flying energy consumption of the UAV is expressed as

$$E_n^f(v_n) = \tau\left(\varsigma_1 v_n^3 + \frac{\varsigma_2}{v_n}\right), \quad \forall n \in \mathcal{N}, \tag{2}$$

where ς_1 and ς_2 are the parameters related to the UAV's weight, air density, wing area, and wing span efficiency, among other factors [19]. The RIS at time slot n is located at $p^R = (x^R, y^R, z^R)$. Accordingly, the Euclidean distances from the RIS to UAV, from the UAV to UE k, and from the UE k to RIS at time slot n are given by $d_n^{RU} = \left\| p^R - p_n^U \right\|$, $d_{k,n}^{UE} = \left\| p_n^U - p_k^E \right\|$, and $d_k^{ER} = \left\| p_k^E - p^R \right\|$, respectively. Each element of the RIS is represented as $m \in \mathcal{M} = \{1, ..., M\}$, and the RIS phase-shift matrix at time slot n is defined as

$$\boldsymbol{\Theta}_n = \mathrm{diag}\left(e^{j\theta_{1,n}}, ..., e^{j\theta_{M,n}}\right), \quad \forall n \in \mathcal{N}, \tag{3}$$

where $j = \sqrt{-1}$ and $\theta_{m,n} \in [0, 2\pi)$ is the phase shift for $\forall m \in \mathcal{M}$ and $\forall n \in \mathcal{N}$.

All entities are assumed to have the known perfect channel state information (CSI). However, the proposed design can be applied to an entity with an imperfect CSI, e.g., the norm-bounded error model [20]. The channels of RIS-to-UAV and UAV-to-UE links are assumed to be dominated by the LOS paths [21] and spatially uncorrelated where the elements in the RIS are linearly separated with a greater than half-wavelength element spacing [22]. Therefore, the channel gain of the RIS-to-UAV links at time slot n is expressed as

$$\boldsymbol{h}_n^{RU}\left(\boldsymbol{p}_n^U\right) = \sqrt{\frac{\beta_0}{\left(d_n^{RU}\right)^2}}\left[1, e^{-j\frac{2\pi d}{\lambda}\phi_n^{RU}}, ..., e^{-j\frac{2\pi(M-1)d}{\lambda}\phi_n^{RU}}\right]^T, \quad \forall n \in \mathcal{N}, \tag{4}$$

where β_0 is the path loss at the reference distance $D_0 = 1$ m, d is the distance between the reflecting elements, λ is the carrier wavelength, and $\phi_n^{RU} = (x^R - x_n^U)/d_n^{RU}$ is the cosine of the angle of departure (AoD) of the signal from the RIS to the UAV. The channel gains of the UAV-to-UE links at time slot n are given by

$$h_{k,n}^{UE}\left(\boldsymbol{p}_n^U\right) = \sqrt{\frac{\beta_0}{\left(d_{k,n}^{UE}\right)^\zeta}}, \quad \forall n \in \mathcal{N} \text{ and } \forall k \in \mathcal{K}, \tag{5}$$

where ζ is the path loss exponent of the UAV-to-UE link for the UE. The channels of the UE-to-RIS links are assumed to follow spatially uncorrelated Rayleigh fading, which yields the channel gain of the UE-to-RIS at time slot n, expressed as follows:

$$\boldsymbol{h}_k^{ER} = \sqrt{\frac{\beta_0}{\left(d_k^{ER}\right)^\epsilon}}\left[1, e^{-j\frac{2\pi d}{\lambda}\phi_k^{ER}}, ..., e^{-j\frac{2\pi(M-1)d}{\lambda}\phi_k^{ER}}\right]^T \xi_k^{ER}, \quad \forall k \in \mathcal{K}, \tag{6}$$

where ϵ is the path loss exponent of the UE-to-RIS link for the UE, $\phi_k^{ER} = (x_k^E - x^R)/d_k^{ER}$ is the cosine of the AoD of the signal from the RIS to UE k, and ξ_k^{ER} is a circularly symmetric complex Gaussian (CSCG) random variable with zero mean and unit variance, which models the random scattering component. Consequently, the effective uplink channel gain from UE k to the UAV at time slot n can be represented as

$$h_{k,n}\left(\boldsymbol{p}_n^U, \boldsymbol{\Theta}_n\right) = h_{k,n}^{UE}\left(\boldsymbol{p}_n^U\right) + \left(\boldsymbol{h}_n^{RU}\left(\boldsymbol{p}_n^U\right)\right)^H \boldsymbol{\Theta}_n \boldsymbol{h}_k^{ER}, \quad \forall n \in \mathcal{N} \text{ and } \forall k \in \mathcal{K}. \tag{7}$$

2.3. Phase for Wireless Energy Transfer (WET)

For WET, the battery of the UE is assumed to have sufficient storage space for saving the harvested energy. The energy signal is transmitted from the UAV to the UE via downlink communication. By leveraging the principle of channel reciprocity, we can denote the downlink channels using (7). The RIS phase-shift matrix and channel gain for UE k at time slot n are defined as $\Theta_n^E = \mathrm{diag}(e^{j\theta_{1,n}^E}, ..., e^{j\theta_{M,n}^E})$ and $h_{k,n}^E(\boldsymbol{p}_n^U, \Theta_n^E)$, respectively. With the transmit power P_n^E for energy harvesting at the UAV, the energy harvested at UE k at time slot n can be calculated as follows:

$$E_{k,n}^H\left(\mu_n, \boldsymbol{p}_n^U, \Theta_n^E, P_n^E\right) = \eta\mu_n\tau P_n^E\left|h_{k,n}^E\left(\boldsymbol{p}_n^U, \Theta_n^E\right)\right|^2, \quad \forall n \in \mathcal{N} \text{ and } \forall k \in \mathcal{K}, \tag{8}$$

where $\eta \in (0, 1]$ is the energy conversion efficiency. Note that the energy harvested at each UE is supposed to be higher than that needed for its operation.

2.4. Phase for Local Computing and Offloading (LO)

We assume that a portion of the computation task can be offloaded to the UAV, and the remainder is processed locally at the UE. Here, the computation task that UE k has to process is denoted as $L_{k,n}$ bits at time slot n. In the LO phase, the UE can execute offloading and local computation simultaneously. For the LO phase, we represent the RIS phase-shift matrix and channel gain for UE k at time slot n as $\Theta_n^I = \mathrm{diag}(e^{j\theta_{1,n}^I}, ..., e^{j\theta_{M,n}^I})$ and $h_{k,n}^I(\boldsymbol{p}_n^U, \Theta_n^I)$, respectively.

Specifically, for multiple access of the offloaded data via the uplink, the RSMA method is used [23,24]. The RSMA splits user messages by partially decoding interference and treating interference as noise via optimal decoding, resulting in effective power control and high spectral efficiency. The transmitted signal $s_{k,n}^u$ of each UE k at time slot n is split into two submessages for the RSMA method, which is given by

$$x_{k,n} = \sum_{s=1}^{2} \sqrt{P_{l,n,j}} s_{k,n,s}, \quad \forall n \in \mathcal{N} \text{ and } \forall k \in \mathcal{K}, \tag{9}$$

where the transmit power of the subsignal $s_{k,n,s}$ at time slot n is represented as $P_{k,n,s}$. The submessages of the UEs are divided based on the split proportion $a_{k,n,s}$, and submessages with higher proposition indices have a higher priority compared with other submessages, which satisfies

$$R_{k,n,1}\left(\boldsymbol{p}_n^U, \Theta_n^I, P_{k,n,1}\right) : R_{k,n,2}\left(\boldsymbol{p}_n^U, \Theta_n^I, P_{k,n,2}\right) = a_{k,n,1} : a_{k,n,2}, \quad \forall n \in \mathcal{N} \text{ and } \forall k \in \mathcal{K}. \tag{10}$$

Using the predetermined proportion index for UE k, the submessages can be prioritized based on their known proportional index information. The total received signal at time slot n can be represented as follows:

$$y_n = h_{k,n}^I\left(\boldsymbol{p}_n^U, \Theta_n^I\right) \sum_{k=1}^{K} \sum_{s=1}^{2} \sqrt{P_{k,n,s}} s_{k,n,s} + n_0, \quad \forall n \in \mathcal{N} \text{ and } \forall k \in \mathcal{K}, \tag{11}$$

where n_0 is the additive white Gaussian noise at the UAV that satisfies $\mathcal{CN}(0, \sigma^2)$. At the UAV, all the subsignals are decoded using the successive interference cancellation (SIC) technique, where the decoding order is denoted by $\pi_n = \{\pi_{1,n,1}, ..., \pi_{k,n,s}, ..., \pi_{K,n,2}\}$, with $\pi_{k,n,s} \in \{1, 2, ..., 2K\}$ being the decoding order of the subsignal s of UE k at the nth time slot

to be predetermined. Thus, the achievable uplink rate of the subsignal $s_{k,n,s}$ at time slot n is given by

$$R_{k,n,s}\left(\boldsymbol{p}_n^U, \boldsymbol{\Theta}_n^I, P_{k,n,s}\right) = \mathrm{B}\log_2\left(1 + \frac{P_{k,n,s}\left|h_{k,n}^I\left(\boldsymbol{p}_n^U, \boldsymbol{\Theta}_n^I\right)\right|^2}{\sum_{\pi_{l,n,j} > \pi_{k,n,s}} P_{l,n,j}\left|h_{l,n}^I\left(\boldsymbol{p}_n^U, \boldsymbol{\Theta}_n^I\right)\right|^2 + \sigma^2}\right), \quad (12)$$

for $\forall n \in \mathcal{N}$ and $\forall k \in \mathcal{K}$, where B is the system bandwidth and $\pi_{l,n,j}$ is the decoding order of the subsignal j of UE l. The total achievable rate of UE k is

$$R_{k,n}\left(P_{k,n,s}, \boldsymbol{p}_n^U, \boldsymbol{\Theta}_n^I\right) = \sum_{s=1}^2 R_{k,n,s}\left(\boldsymbol{p}_n^U, \boldsymbol{\Theta}_n^I\right), \quad \forall n \in \mathcal{N}, \ \forall k \in \mathcal{K} \text{ and } s \in \{1,2\}. \quad (13)$$

The energy consumption of UE k at time slot n for transferring the offloaded data is calculated as

$$E_{k,n}^o(P_{k,n,s}) = (1 - \mu_n)\tau \sum_{s=1}^2 P_{k,n,s}, \quad \forall n \in \mathcal{N} \text{ and } \forall k \in \mathcal{K}. \quad (14)$$

When the offloaded bits from UE k to the UAV is denoted as $L_{k,n}^o$, we have

$$L_{k,n}^o \leq (1 - \mu_n)\tau R_{k,n}\left(\boldsymbol{p}_n^U, \boldsymbol{\Theta}_n^I, P_{k,n,s}\right), \quad \forall n \in \mathcal{N} \text{ and } \forall k \in \mathcal{K}. \quad (15)$$

After offloading $L_{k,n}^o$ bits, the remaining $L_{k,n} - L_{k,n}^o$ bits need to be processed by local computing at UE k. The number of CPU cycles per input bit required for UE k to compute is C_k, and the number of CPU cycles required for UE k to compute locally at time slot n is $C_k(L_{k,n} - L_{k,n}^o)$. We adopt dynamic voltage and frequency scaling (DVFC) by referring ot a previous study [1]. By adjusting the CPU frequency $f_{k,n}^q$ for the qth CPU cycle, UE k can control the amount of energy used for executing the tasks locally, where $q \in \{1, ..., C_k(L_{k,n} - L_{k,n}^o)\}$, $f_{k,n}^q \in (0, f_k^{\text{high}}]$, and $f_{k,n}^{\text{high}}$ is the highest CPU frequency of UE k. UE k has to complete local computing during $(1 - \mu_n)\tau$, i.e.,

$$\sum_{q=1}^{C_k(L_{k,n} - L_{k,n}^o)} \frac{1}{f_{k,n}^q} \leq (1 - \mu_n)\tau, \quad \forall n \in \mathcal{N} \text{ and } \forall k \in \mathcal{K}, \quad (16)$$

where $\sum_{q=1}^{C_k(L_{k,n} - L_{k,n}^o)} 1/f_{k,n}^q$ is the total execution time of the local computing process at UE k. The energy consumption of UE k at time slot n for local computing is therefore calculated as

$$E_{k,n}^l\left(L_{k,n}^o, f_{k,n}^q\right) = \sum_{q=1}^{C_k(L_{k,n} - L_{k,n}^o)} \kappa\left(f_{k,n}^q\right)^2, \quad \forall n \in \mathcal{N} \text{ and } \forall k \in \mathcal{K}, \quad (17)$$

where κ is the energy efficiency coefficient of the CPU architecture [5].

2.5. Phases for UAV Computing and Downloading

The linear simplified model is used to evaluate the computing energy of the UAV [5]. The computing energy consumption of the UAV is then given by

$$E_n^c(L_{k,n}^o) = \varphi \sum_{k=1}^K L_{k,n}^o, \quad \forall n \in \mathcal{N} \text{ and } \forall k \in \mathcal{K}. \quad (18)$$

The time required for UAV computing and downloading the offloading results is assumed to be negligible due to the UAV's high capability and the small output data size [5].

3. Energy Minimization in RIS-Assisted UAV-Enabled WP-MEC with RSMA

3.1. Problem Formulation

We aim at minimizing the total energy consumption by jointly optimizing the time allocation $\{\mu_n\}$ for the WET and LO phases, power allocation $\{P_n^E\}$ for the WET phase, power allocation $\{P_{k,n,s}\}$ for the LO phase, UAV trajectory $\{p_n^U, v_n\}$, RIS's phase-shift matrix $\{\Theta_n^E, \Theta_n^I\}$, the task size at each time slot $\{L_{k,n}\}$, the task size of computation offloading $\{L_{k,n}^o\}$, and CPU frequencies k $\{f_{k,n}^q\}$. The total energy consumption of the system can be expressed as

$$E^{\text{tot}}(\mu, P, L, v) = \sum_{n=1}^{N} \left(E_n^E(\mu_n, P_n^E) + E_n^c(L_{k,n}^o) + E_n^f(v_n) \right) + E_c, \tag{19}$$

where $\mu \triangleq \{\mu_n\}_{n\in\mathcal{N}}$, $P \triangleq \{P_n^E, P_{k,n,s}\}_{n\in\mathcal{N},k\in\mathcal{K},s\in\{1,2\}}$, $v \triangleq \{v_n\}_{n\in\mathcal{N}}$, $L \triangleq \{L_{k,n}, L_{k,n}^o\}_{n\in\mathcal{N},k\in\mathcal{K}}$, $E_n^E(\mu_n, P_n^E) = \mu_n \tau P_n^E$, and E_c denotes the energy consumed by the circuit and control at the UAV and RIS, which is usually a fixed value that can be ignored. Thus, the energy minimization problem is formulated as follows:

$$\min_{\{\mu, P, p^U, v, \Theta, f, L\}} E^{\text{tot}}(\mu, P, L, v) \tag{20a}$$

$$\text{s.t.} \quad (1), (10), (15), (16), \tag{20b}$$

$$L_k^{tot} \leq \sum_{n=1}^{N} L_{k,n}, \quad \forall k \in \mathcal{K}, \tag{20c}$$

$$0 \leq L_{k,n} - L_{k,n}^o \leq \frac{(1-\mu_n)\tau f_k^{\text{high}}}{C_k}, \quad \forall n \in \mathcal{N} \text{ and } \forall k \in \mathcal{K}, \tag{20d}$$

$$\sum_{i=1}^{n} \left(E_{k,i}^o + E_{k,i}^l \left(L_{k,i}^o, f_{k,i}^q \right) \right) \leq \sum_{i=1}^{n} E_{k,i}^H \left(\mu_i, p_i^U, \Theta_i^E, P_i^E \right), \quad \forall n \in \mathcal{N} \text{ and } \forall k \in \mathcal{K}, \tag{20e}$$

$$0 \leq \mu_n \leq 1, \quad \forall n \in \mathcal{N}, \tag{20f}$$

$$0 \leq \theta_{m,n}^E \leq 2\pi, \quad 0 \leq \theta_{m,n}^I \leq 2\pi, \quad \forall n \in \mathcal{N} \text{ and } \forall m \in \mathcal{M}, \tag{20g}$$

$$0 \leq f_{k,n}^q \leq f_k^{\text{high}}, \quad \forall n \in \mathcal{N} \text{ and } \forall k \in \mathcal{K}, \tag{20h}$$

$$P_n^E, P_{k,n,s}, L_{k,n}, L_{k,n}^o \geq 0, \quad \forall n \in \mathcal{N} \text{ and } \forall k \in \mathcal{K} \text{ and } s \in \{1,2\}, \tag{20i}$$

$$p_1^U = p_I^U, \quad p_N^U = p_F^U. \tag{20j}$$

where $p^U \triangleq \{p_n^U\}_{n\in\mathcal{N}}$, $\Theta \triangleq \{\Theta_n^E, \Theta_n^I\}_{n\in\mathcal{N}}$, and $f \triangleq \{f_{k,n}^q\}_{n\in\mathcal{N},k\in\mathcal{K}}$. The constraint (20c) is for the total bits to be calculated; (20d) bounds locally computed tasks such that they do not exceed the maximum CPU frequency that can be processed during the LO phase; (20e) is the energy harvesting constraint that the harvested energy has to be larger than or equal to the total energy consumption of the UE; (20f) bounds the time allocation for the WET and the LO phases; (20g) and (20i) are non-negative constraints of the RIS phase shift, power allocation, and offloading task size; (20h) bounds the CPU frequency of UE k; and (1) and (20j) guarantee the valid path of the UAV. As the objective function (20a) and constraints (10), (15), (16) and (20e) are nonconvex, the problem (20) is nonconvex.

3.2. Proposed Algorithm

Herein, we propose an algorithm that obtains the local optimal solution for the energy minimization problem (20). Due to the coupling of the optimization variables, the AO-based approach is used herein. Specifically, we derive the semiclosed-form solution for

local CPU frequencies and obtain the remaining optimization variables of (20) using the AO algorithm.

3.2.1. Optimization of Local CPU Frequency

The following lemma (Lemma 1) is developed by referring to a previous study [5] to determine the local CPU frequency of the UE.

Lemma 1. *Given the number of bits to be computed, the ideal local CPU frequencies of the UE required to minimize the computing energy consumption are given as*

$$f_{k,n}^1 = f_{k,n}^2 = \cdots = f_{k,n}^{C_k(L_{k,n} - L_{k,n}^o)} = \frac{C_k\left(L_{k,n} - L_{k,n}^o\right)}{(1 - \mu_n)\tau}, \quad \forall n \in \mathcal{N} \text{ and } \forall k \in \mathcal{K}. \quad (21)$$

For energy minimization, as indicated in equation (17), the energy calculation is directly proportional to the square of the frequency. Accordingly, the optimal results can be achieved by assigning the same frequency to all CPU cycles. Based on Lemma 1 and using the optimal frequencies of the UE, the problem (20) can be reformulated as

$$\min_{\{\mu, P, p^U, v, \Theta, L\}} E^{\text{tot}}(\mu, P, L, v) \tag{22a}$$

$$\text{s.t.} \quad (1), (10), (15), (20c), (20d), (20f), (20g), (20i), (20j) \tag{22b}$$

$$\sum_{i=1}^n \left(E_{k,i}^o(P_{k,n,s}) + \frac{\kappa C_k^3\left(L_{k,i} - L_{k,i}^o\right)^3}{(1 - \mu_i)^2 \tau^2} \right) \leq \sum_{i=1}^n E_{k,i}^H\left(\mu_i, p_i^U, \Theta_i^I, P_i^E\right), \tag{22c}$$

for $\forall n \in \mathcal{N}$ and $\forall k \in \mathcal{K}$.

3.2.2. Optimization of Transmit Power and Bit Allocation

Given the time ratio μ, the UAV trajectory p^U, and the RIS phase shift Θ, the subproblem for optimizing the uplink and downlink transmit powers P and offloaded bit L can be represented as

$$\min_{\{P, L\}} \sum_{n=1}^N \left(E_n^E(\mu_n, P_n^E) + E_n^c(L_{k,n}^o) \right) \tag{23a}$$

$$\text{s.t.} \quad (10), (15), (20c), (20d), (20i), (22c). \tag{23b}$$

This problem is nonconvex due to the constraints (10) and (15). Using the constraint (10), the constraint (15) is equivalently written as

$$\frac{a_{k,n,s} L_{k,n}^o}{(1 - \mu_n)\tau} \leq R_{k,n}\left(p_n^U, \Theta_n^I, P_{k,n,s}\right), \quad \forall n \in \mathcal{N} \text{ and } \forall k \in \mathcal{K}. \tag{24}$$

Successive convex approximation (SCA) is used to handle this constraint [9,25], which can approximately solve a nonconvex problem by converting it into a sequence of convex subproblems. In this technique, the nonconvex objective function and constraints are replaced with suitable convex approximations, enabling iterative problem solution iterations. Then, the right side of (24) can be written as

$$R_{k,n,s}\left(\boldsymbol{p}_n^U, \boldsymbol{\Theta}_n^I, P_{k,n,s}\right)$$

$$= \mathrm{B}\log_2\left(1 + \frac{P_{k,n,s}\left|h_{k,n}^I\left(\boldsymbol{p}_n^U, \boldsymbol{\Theta}_n^I\right)\right|^2}{\sum_{\pi_{l.n.j} > \pi_{k,n,s}} P_{l,n,j}\left|h_{l,n}^I\left(\boldsymbol{p}_n^U, \boldsymbol{\Theta}_n^I\right)\right|^2 + \sigma^2}\right)$$

$$= \mathrm{B}\log_2\left(\sum_{\pi_{l.n.j} \geq \pi_{k,n,s}} P_{l,n,j}|h_{l,n}^I(\boldsymbol{p}_n^U, \boldsymbol{\Theta}_n^I)|^2 + \sigma^2\right) - \mathrm{B}\log_2\left(\sum_{\pi_{l.n.j} > \pi_{k,n,s}} P_{l,n,j}|h_{l,n}^I(\boldsymbol{p}_n^U, \boldsymbol{\Theta}_n^I)|^2 + \sigma^2\right)$$

$$\geq \mathrm{B}\log_2\left(\sum_{\pi_{l.n.j} \geq \pi_{k,n,s}} P_{l,n,j}|h_{l,n}^I(\boldsymbol{p}_n^U, \boldsymbol{\Theta}_n^I)|^2 + \sigma^2\right) - \mathrm{B}\log_2\left(\sum_{\pi_{l.n.j} > \pi_{k,n,s}} P_{l,n,j}^{(z)}|h_{l,n}^I(\boldsymbol{p}_n^U, \boldsymbol{\Theta}_n^I)|^2 + \sigma^2\right)$$

$$- \frac{\sum_{\pi_{l.n.j} > \pi_{k,n,s}} |h_{l,n}^I(\boldsymbol{p}_n^U, \boldsymbol{\Theta}_n^I)|^2(P_{l,n,j} - P_{l,n,j}^{(z)})}{\left(\sum_{\pi_{l.n.j} > \pi_{k,n,s}} P_{l,n,j}^{(z)}|h_{l,n}^I(\boldsymbol{p}_n^U, \boldsymbol{\Theta}_n^I)|^2 + \sigma^2\right)\log(2)} \triangleq \hat{R}_{k,n,s'}^P \tag{25}$$

where $P_{k,n,s}^{(z)}$ is the local point at iteration z. Accordingly, the problem (22) can be transformed as

$$\min_{\{\boldsymbol{P}, \boldsymbol{L}\}} \sum_{n=1}^N \left(E_n^E(\mu_n, P_n^E) + E_n^c(L_{k,n}^o)\right) \tag{26a}$$

$$\text{s.t.} \quad (20c), (20d), (20i). (22c) \tag{26b}$$

$$\frac{a_{k,n,s}L_{k,n}^o}{(1-\mu_n)\tau} \leq \tilde{R}_{k,n,s'}^P \quad \forall n \in \mathcal{N} \text{ and } \forall k \in \mathcal{K}. \tag{26c}$$

(26) is a convex problem that can be easily solved using the standard mathematical convex optimization method or a toolbox such as CVX [25,26].

3.2.3. Optimization of the UAV's Trajectory and RIS's Phase Shift

The RIS phase shift $\boldsymbol{\Theta}$ and UAV trajectory $\{\boldsymbol{p}^U, \boldsymbol{v}\}$ are optimized for the given remaining variables $\boldsymbol{\mu}$, $\boldsymbol{P}$, and $\boldsymbol{L}$ using the AO approach. The same phase-shift design for the RIS in uplink and downlink can guarantee satisfactory performance [27,28], i.e., $\Theta_n^I = \Theta_n^E = \Theta_n$. By channel modeling (4), (6) and (7), the reflective channel gain $(\boldsymbol{h}_n^{RU}(\boldsymbol{p}_n^U))^H \Theta_n \boldsymbol{h}_k^{ER}$ can be rewritten as

$$h_{k,n}\left(\boldsymbol{p}_n^U, \boldsymbol{\Theta}_n\right) = \left(\boldsymbol{h}_n^{RU}\left(\boldsymbol{p}_n^U\right)\right)^H \boldsymbol{\Theta}_n \boldsymbol{h}_k^{ER} = \frac{\beta_0}{d_n^{RU}\left(d_k^{ER}\right)^{\epsilon/2}} \sum_{m=1}^M e^{j\psi_{m,k}^{UE}}, \tag{27}$$

where $\psi_{m,k}^{UE} = \theta_{m,n} + \frac{2\pi}{\lambda}\left(d(m-1)(\phi_k^{ER} - \phi_n^{RU})\right) + \arg\left(\xi_k^{ER}\right)$. When the signals from different paths are combined coherently at the UE and UAV, the received signal power is maximized. As $h_{k,n}^{UE}$ is a real value (7), if $\psi_{m,k}^{UE} = \arg\left(h_{k,n}^{UE}\right) = 0$, the achievable uplink rate $R_{k,n}^u$ and the harvested energy $E_{k,n}^H$ can be maximized. Accordingly, the optimal phase shift of the RIS at time slot n can be expressed as follows:

$$\theta_{m,n} = \frac{2\pi}{\lambda}\left(d(m-1)(\phi_n^{RU} - \phi_k^{ER})\right), \quad \forall n \in \mathcal{N} \text{ and } \forall m \in \mathcal{M}. \tag{28}$$

Based on the phase design of the RIS in (28), the trajectory of the UAV needs to be designed.

Thus, the effective channel gain for UE k at time slot n can be rewritten as

$$h_{k,n}\left(p_n^U\right) = \sqrt{\frac{\beta_0}{\left(d_{k,n}^{UE}\right)^\zeta} + \frac{\beta_0 M}{d_n^{RU}\left(d_k^{ER}\right)^{\epsilon/2}}}, \quad \forall n \in \mathcal{N} \text{ and } \forall k \in \mathcal{K}. \tag{29}$$

Using the proposed phase design Θ in (28), the subproblem for the UAV's trajectory design is expressed as

$$\min_{p^U, v} \quad \sum_{n=1}^{N} \left(E_n^f(v_n)\right) \tag{30a}$$

$$\text{s.t.} \quad (1), (24), (20j), (22c). \tag{30b}$$

As the objective function (30) and the constraints (22c), and (24) are nonconvex, the SCA method is applied by introducing the slack variables $\tilde{v} = \{\tilde{v}_n\}_{\forall n}$, $u = \{u_{k,n}\}_{\forall k,n}$, $w = \{w_n\}_{\forall n}$, and $t = \{t_{k,n}\}_{\forall k,n}$, which yield the following convex problem:

$$\min_{\{p^U, v, \tilde{v}, u, w, t\}} \quad \sum_{n=1}^{N} \left(\tilde{E}_n^f(v_n, \tilde{v}_n)\right) \tag{31a}$$

$$\text{s.t.} \quad (1), (20j), (A3) \tag{31b}$$

$$t_{k,n} \le \hat{h}_{k,n}, \quad \forall n \in \mathcal{N} \text{ and } \forall k \in \mathcal{K} \tag{31c}$$

$$\frac{a_{k,n,s} L_{k,n}^o}{(1 - \mu_n)\tau} \le \hat{R}_{k,n,s}^U, \quad \forall n \in \mathcal{N} \text{ and } \forall k \in \mathcal{K} \text{ and } s \in \{1, 2\} \tag{31d}$$

$$\sum_{i=1}^{n} \left(E_{k,i}^o(P_{k,n,s}) + \frac{\kappa C_k^3 (L_{k,i} - L_{k,i}^o)^3}{(1 - \mu_i)^2 \tau^2}\right) \le \eta \mu_n \tau P_n^E \hat{h}_{k,n}, \quad \forall n \in \mathcal{N} \text{ and } \forall k \in \mathcal{K}. \tag{31e}$$

The derivations of (31) are detailed in Appendix A. Algorithm 1 is used to obtain the solution of the problem (31), which can be readily solved using CVX (version 2.2) [25,26].

Algorithm 1 UAV's Trajectory Optimization

Input: Initialize $z(0) = \{z_n(0)\}_{n \in \mathcal{N}} \in \mathcal{X}$ with $\{z_n(0)\}_{n \in \mathcal{N}} \triangleq (p_n^{U(z)}, \{u_{k,n}^{(z)}\}_{k \in \mathcal{K}}, w_n^{(z)})$, $\{\tilde{v}_n\}_{n \in \mathcal{N}}$, $\{v_n\}_{n \in \mathcal{N}}$ fixed μ, P, Θ, L. Set $l = 0$
Repeat: Until the convergence criterion is satisfied.
  Obtain Θ^* using (28) for given $p^{U(z)}$.
  Find $(z^*(z^{(z)}), v^*)$ using the solution of the problem (31).
  Set $z(l + 1) = z^{(z)} + \alpha^{(z)}(z^*(z^{(z)}) - z^{(z)})$ for some $\alpha^{(z)} \in (0, 1]$.
  Update $z \leftarrow z + 1$
Output: p^{U*}, v^*

3.2.4. Optimization of Time Ratio

Given the uplink and downlink power P, the UAV's trajectory $\{p^U, v\}$, the RIS's phase shift Θ, and the offloaded bit L, the subproblem for the time ratio μ can be formulated as follows:

$$\min_{\mu} \sum_{n=1}^{N} \left(E_n^E(\mu_n, P_n^E)\right) \tag{32a}$$

$$\text{s.t.} \quad (20f), (20d), (22c), (24). \tag{32b}$$

Due to its convexity, the solution to problem (32) can be readily obtained using CVX [25,26].

3.3. Overall Algorithm

Algorithm 2 is used for energy minimization in the RIS-assisted UAV-enabled WP-MEC system to achieve a high-quality local optimal solution of problem (20). Specifically, in each iteration k of the proposed Algorithm 2, we consider three subproblems of the original problem (20): (1) optimization of $P(k+1)$ and $L(k+1)$ with fixed $\mu(k)$, $\Theta(k)$, $p^U(k)$, and $v(k)$ using (26); (2) optimization of $\Theta(k+1)$, $p^U(k+1)$, and $v(k+1)$ with fixed $\mu(k)$, $P(k+1)$, and $L(k+1)$ using Algorithm 1 for problem (31); and (3) optimization of $\mu(k+1)$ with fixed $\Theta(k+1)$, $p^U(k+1)$, $v(k+1)$, $P(k+1)$, and $L(k+1)$ using problem (32).

The subproblems (26) and (31) introduced in Sections 3.2.2 and 3.2.3 adopt the bounds for substituting the nonconvex objective function or constraints with their convex approximations, such as (26c), (31a), (31d), and (31e). By solving each subproblem and updating the variables to be optimized, the optimal variables are iteratively obtained in Algorithm 2 based on the AO approach [29]. In Algorithm 1, to optimize the UAV's trajectory (Section 3.2.2), the *l*th solution of the optimization variables, i.e., $z(l)$, is bounded, and $z(\infty)$ has a stationary solution for problem (31) if the step size $\alpha^{(z)}$ is under $\alpha^{(z)} \in (0,1]$, $\alpha^{(z)} \to 0$, and $\sum_z \alpha^{(z)} = \infty$ [30]. Accordingly, the convergence of Algorithm 2 is guaranteed by obtaining the feasible solution in the convex problem based on the bounds with the initial values in the feasible set of each subproblem [30,31]. In addition, the convergence of the proposed Algorithm 2 is numerically verified in terms of the total energy consumption of the UAV (Figure 3).
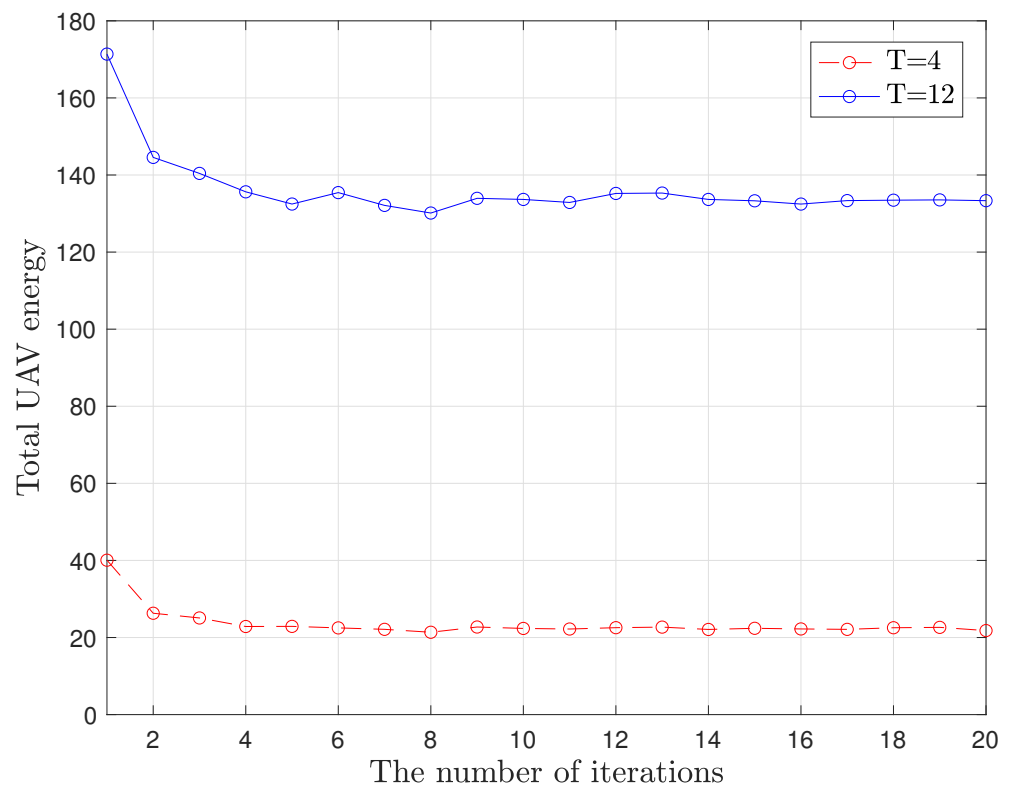

Figure 3. Total energy consumption of the UAV obtained using the proposed Algorithm 2 versus the number of iterations ($M = 16$).

The computational complexity of the proposed algorithm can be analyzed by the complexity of three subproblems in each iteration. In subproblem (26), $3KN + N$ variables are optimized using the convex solver in terms of transmit power $P(k+1)$ and bit allocation $L(k+1)$ with the computational complexity $\mathcal{O}((3KN + N)^{3.5})$. Moreover, as subproblem (31) has an inner iteration loop in Algorithm 1 for obtaining the optimal UAV's trajectory, the computational complexity is calculated as $\mathcal{O}(N_1(KN + 4N)^{3.5})$ with N_1 inner iterations. In addition, the computational complexity for subproblem (32) is represented as $\mathcal{O}(N^{3.5})$.

Therefore, the total complexity of the proposed algorithm is calculated as $\mathcal{O}(N_2 N_1 (KN)^{3.5})$, where N_2 is the number of iterations in Algorithm 2.

Algorithm 2 Algorithm for energy minimization in the RIS-assisted UAV-enabled WP-MEC system

---

Input: Initialize $\boldsymbol{\mu}(0), \boldsymbol{P}(0), \boldsymbol{p}^U(0), \boldsymbol{v}(0), \boldsymbol{\Theta}(0), \boldsymbol{L}(0)$. Set $k = 0$
Repeat: Until the convergence criterion is satisfied.
  Obtain $\boldsymbol{P}(k+1)$ and $\boldsymbol{L}(k+1)$ using the solution of the problem (26) for given $\boldsymbol{\mu}(k), \boldsymbol{\Theta}(k)$, $\boldsymbol{p}^U(k)$, and $\boldsymbol{v}(k)$.
  Obtain $\boldsymbol{\Theta}(k+1), \boldsymbol{p}^U(k+1)$, and $\boldsymbol{v}(k+1)$ from Algorithm 1 for given $\boldsymbol{\mu}(k), \boldsymbol{P}(k+1)$, and $\boldsymbol{L}(k+1)$.
  Obtain $\boldsymbol{\mu}(k+1)$ using the solution of the problem (32) for given $\boldsymbol{\Theta}(k+1), \boldsymbol{p}^U(k+1)$, $\boldsymbol{v}(k+1), \boldsymbol{P}(k+1)$, and $\boldsymbol{L}(k+1)$.
  Update $k \leftarrow k+1$
Output: $\boldsymbol{\mu}^*, \boldsymbol{P}^*, \boldsymbol{p}^{U*}, \boldsymbol{v}^*, \boldsymbol{\Theta}^*, \boldsymbol{L}^*$

---

4. Numerical Results

The performance of Algorithm 2 to jointly optimize the local CPU frequency f, the uplink and downlink power $\boldsymbol{P}$, the bit allocation $\boldsymbol{L}$, the UAV's trajectory $\{\boldsymbol{p}^U, \boldsymbol{v}\}$, the RIS's phase shift $\boldsymbol{\Theta}$, and the time ratio $\boldsymbol{\mu}$ is investigated via numerical results. Throughout the numerical results, we consider $K = 2$ UEs located at $\boldsymbol{p}_1^E = (-5, 5, 0)$ and $\boldsymbol{p}_2^E = (5, 5, 0)$ and the RIS with M elements located at $\boldsymbol{p}^R = (0, 1, 2)$. The UAV is supposed to fly from $\boldsymbol{p}_I^U = (-10, 0, 5)$ to $\boldsymbol{p}_F^U = (10, 0, 5)$. For simplicity, all UE is considered to have the same amount of data to process. Unless otherwise specified, the remaining parameters for the simulations are given in Table 1 by following [9,10].

Table 1. Configuration of simulation parameters.

Parameters	Values	Parameters	Values
K	2	N	T/τ
τ	0.2	σ^2	-100.98 (dBm)
d	$\lambda/2$	ς_1	0.00614
ς_2	15.976	v_{max}	10 (m/s)
η	0.8	f_k^{high}	1 (GHz)
L_k^{tot}	10^5 (bits)	κ	10^{-28}
φ	10^{-5}	C_k	10^5
ϵ	2.2	ζ	2.2
β_0	0 (dB)	B	20 (MHz)

For reference, the proposed method is compared with five benchmark schemes: (i) no optimization of transmit power and bit allocation (`No_pow&bit_alloc_opt`), where the trajectory $\boldsymbol{p}^U$ of the UAV and the time ratio $\boldsymbol{\mu}$ are obtained using the proposed algorithm, and the equal allocation of transmit power and bit is considered for offloading per interval; (ii) no optimization of the UAV's trajectory (`No_tra_opt`) [4], where the time ratio $\boldsymbol{\mu}$, transmit power $\boldsymbol{P}$, and bit allocation $\boldsymbol{L}$ are optimized using the proposed algorithm, and the UAV flies in a straight line from initial to final positions at a constant velocity; (iii) no optimization of time ratio (`No_time_ratio_opt`), where the time ratio $\mu_k = 0.5$ for all $k \in \mathcal{K}$ is constant, and the UAV's trajectory $\boldsymbol{p}^U$, transmit power $\boldsymbol{P}$, and bit allocation $\boldsymbol{L}$ are optimized using the proposed algorithm; (iv) the proposed algorithm without the RIS (`Proposed algorithm w/o RIS`), where Algorithm 2 is applied to the case without the RIS that has the only direct path of the UAV-to-UE communication link, and therefore, it does not require the RIS's phase-shift design; and (v) the proposed algorithm with orthogonal multiple access (OMA) (`Proposed algorithm w/ OMA`), where the proposed Algorithm 2 is applied for the OMA case. Note that, in the OMA approach, only one message has to

be communicated for each user; therefore, each user is assigned to $1/K$ time or frequency resource to avoid any interference.

First, the convergence of the proposed algorithms is numerically investigated. Figure 3 shows the total energy consumption of the UAV versus the number of iterations obtained by Algorithm 2 with different mission time T, where the number of RIS elements is $M = 16$. Here, the iterations of the proposed algorithm are the outer iterations of Algorithm 2. The proposed algorithm converges quickly in terms of the total energy consumption of the UAV at about 10–14 steps. Moreover, it is observed that the number of iterations required to converge increases with the number of optimized variables, e.g., by considering a large number of slots with a large T.

Figure 4 shows the optimal trajectories of a UAV designed using the proposed algorithm. In Figure 4, the UAV gets closer to the location between the UE and RIS to mitigate the path loss between the UAV and UE, as well as that between the UAV and the RIS. This is because the performances in terms of the harvested energy at the UE in the WET phase and the achievable rate of the UE are inversely and exponentially proportional to the interdistances from the UAV to the UE and to the RIS. However, in the case of a large number of RIS elements, i.e., $M = 1024$, as the path loss of the UE–RIS–UAV link can be sufficiently compensated by the optimized RIS phase shift Θ, the optimal UAV's trajectory can be identical to the benchmark scheme with no optimization of the UAV's trajectory (`No_tra_opt`).
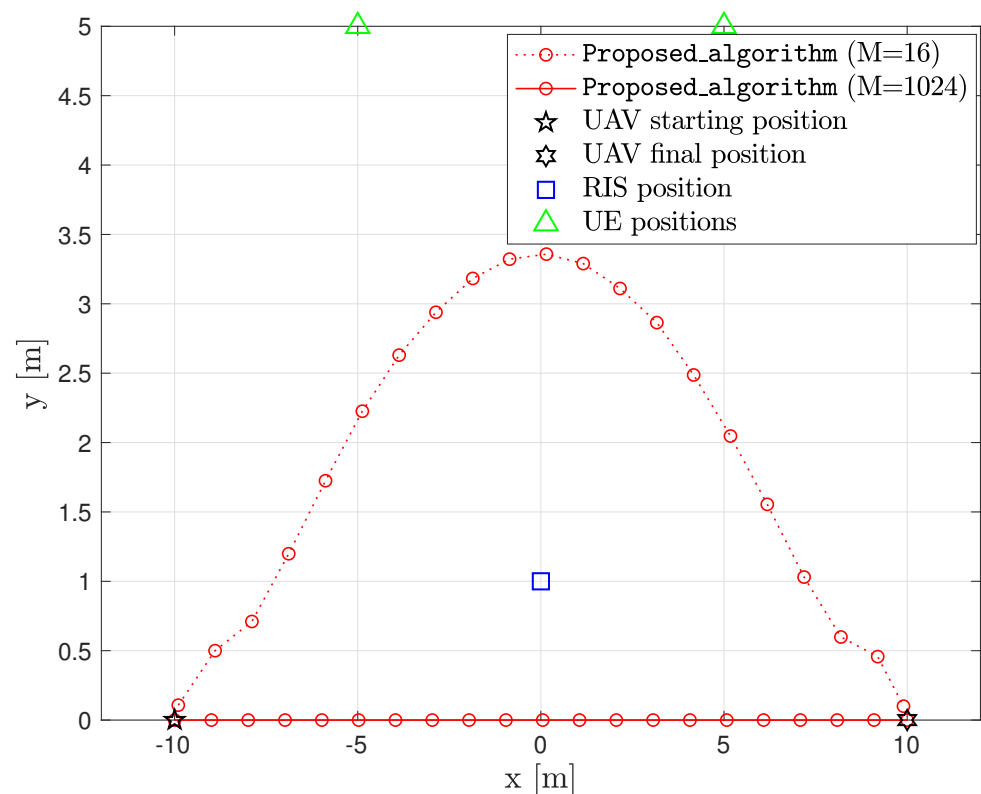

Figure 4. Optimal trajectory of the UAV obtained using the proposed Algorithm 2 ($T = 40$).

The impact of the mission time T on the total energy consumption of the UAV is shown in Figure 5, with the number of RIS elements $M = 16$. It is noticed that the proposed algorithm always outperforms the other benchmark schemes. In addition, the performance of either `No_tra_opt` or `No_time_ratio_opt` is similar to that of the proposed algorithm at a low mission time T. This is because the improvement in performance obtained by optimizing either the UAV's trajectory or time ratio becomes small due to stringent constraints at a low mission time T. In contrast, the energy consumption of the UAV for

the benchmark scheme without the optimization of transmit power and bit allocation (`No_pow&bit_alloc_opt`) approaches that of the proposed algorithm as the mission time T increases. Thus, the significance of the optimal resource allocation is emphasized when the resource for communication and computing, i.e., mission time T, is insufficient. Moreover, as a less-achievable rate for transferring the offloaded data per time slot is required for ensuring sufficient mission time, the performance gain of RSMA decreases compared with that of OMA as the mission time T increases. Oppositely, the performance gap between the cases with and without the RIS exists despite the joint optimization of the energy consumption of the UAV. This can be explained by the reduction in the channel gain resulting from the no-virtual-RIS link in the case without the RIS, which drastically reduced the achievable rate and amount of energy harvested at the UE.
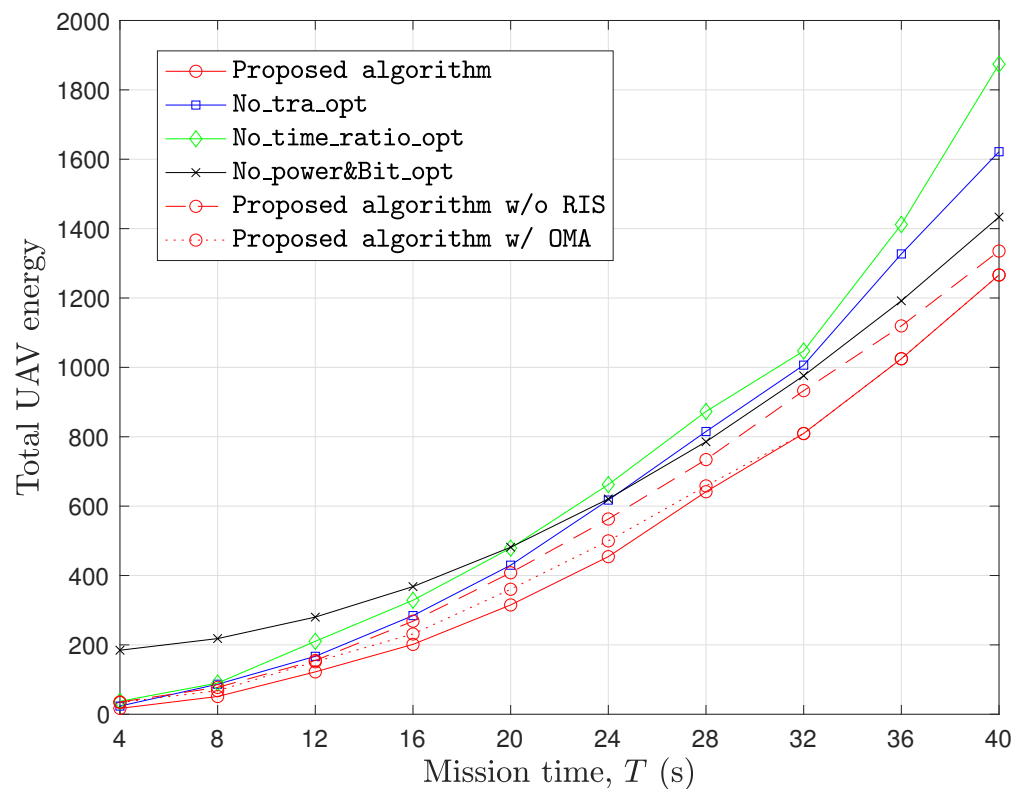
Figure 5. Total energy consumption of the UAV versus the mission time T ($M = 16$).

In Figure 6, the total energy consumption of the UAV is plotted versus the number of RIS elements M at the mission time $T = 25$. Figure 6 shows that the energy consumption of the UAV decreases with an increasing number of RIS elements, M, owing to the improved channel gains that enable better performance of WET and an achievable rate. In particular, the amount of energy harvested at the UE increases with the channel gain at a fixed transmit power P_n^E at the UAV, as shown in (8). The desired channel links can also be elevated by increasing the number of RIS elements M and by designing the flying path of the UAV to move toward the UE or the RIS, as observed in Figure 4. It is also noticeable that, for a small number of RIS elements M, the performance superiority of the proposed algorithm is pronounced compared with other reference schemes. As mentioned above, it is observed that the advantage of RSMA is pronounced for a small number of RIS elements, whereas the advantage of RIS becomes prominent for a large number of RIS elements.
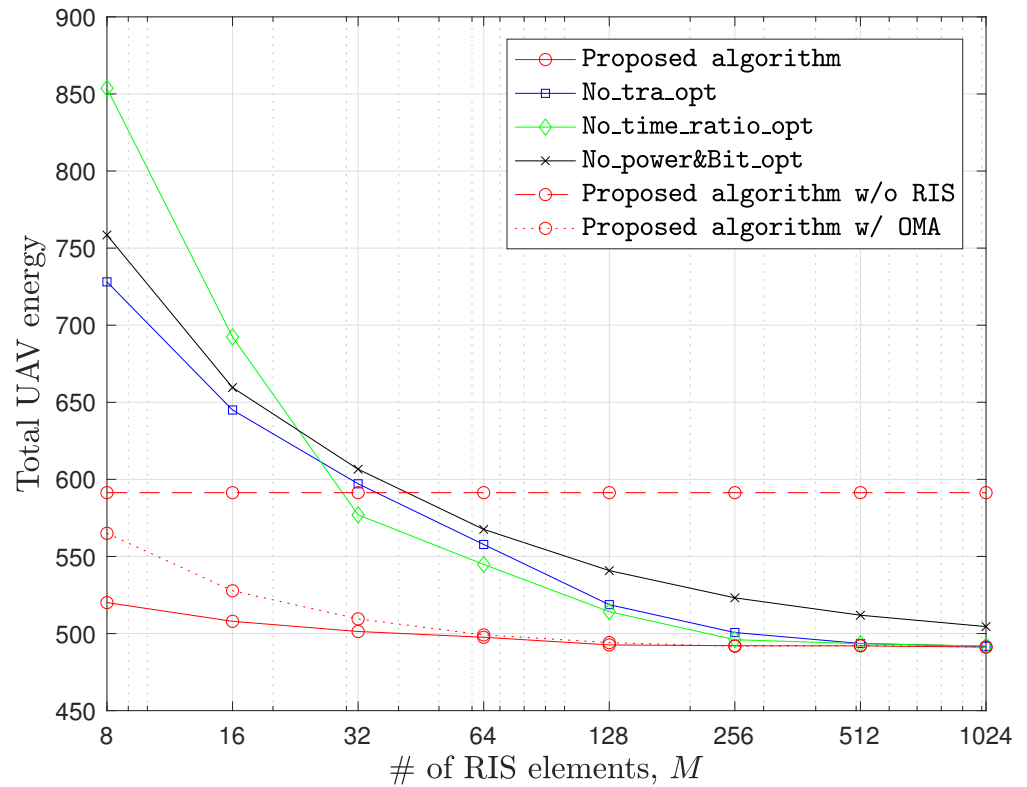
Figure 6. Total energy consumption of the UAV versus the number of RIS elements, M ($T = 25$).

5. Concluding Remarks

A novel RIS-assisted WP-MEC design framework with the aid of a UAV-mounted cloudlet is proposed herein to minimize the total energy consumption of the UAV. By adopting the UAV-mounted cloudlet in order to move freely, the desired channel links can be established for improving the energy efficiency. Simultaneously, as the RIS between the UAV and the UE is deployed, the channel gain can be enhanced thanks to the additional virtual links. The uplink RSMA method is used for improving the spectral efficiency in the offloading procedure of multiple UEs. For realizing WET and MEC, a new frame structure comprising four phases is proposed, such as the (i) WET phase, (ii) local computing and offloading (LO) phase, (iii) UAV's computing phase, and (iv) downloading phase of the computing results. For each phase, we provided detailed operations and related signal models, based on which the energy minimization problem is formulated to jointly optimize resource allocation along with UAV trajectory and the RIS phase-shift matrix. Due to coupling issues between the designs of the optimization variables, an AO-based algorithm is developed to converge to a locally optimal solution, and its convergence and computational complexity are analyzed. Via simulation results, the superiority of the proposed WP-MEC systems and algorithm are verified, and it is revealed that the proposed algorithm reduces the energy consumption to about half of that of the benchmark schemes. This performance gain of the proposed algorithm becomes prominent in the system with insufficient resources, such as a short mission time or a small number of RIS elements. To the best our knowledge, the consideration of both an RIS and UAV-mounted cloudlet for the WP-MEC system has been at the beginning stage of development, and the system performance can be further improved using the RSMA method. The proposed system and algorithm can provide insights into the performances of various 6G system configurations and applications with high computational complexity and low latency, such as extended reality (XR) and remote diagnosis. As future works, the proposed WP-MEC systems can

be extended to a robust design against time offset or imperfect channel state information in asynchronous environments.

Data Availability Statement: Data are contained within the article.

Appendix A. Derivation for (31)

In this appendix, we derive the convex optimization problem (31) for the UAV's trajectory design. To handle the nonconvexity of (30), we employ the upper bound of $E_n^f(\boldsymbol{p}_n^U)$, given as

$$\tilde{E}_n^f(v_n, \tilde{v}_n) = \tau\left(\varsigma_1 v_n^3 + \frac{\varsigma_2}{\tilde{v}_n}\right), \quad \forall n \in \mathcal{N}, \tag{A1}$$

where a slack variable $\tilde{v}_n$ is defined to satisfy the condition $v_n \leq \tilde{v}_n$, which is equivalent to

$$\left\|\boldsymbol{p}_n^U - \boldsymbol{p}_{n-1}^U\right\|^2 \geq \tau^2 \tilde{v}_n^2, \quad \forall n \in \mathcal{N}. \tag{A2}$$

For applying the SCA technique [9,25], we adopt the first-order Taylor expansion at a local point $\boldsymbol{p}_n^{U(z)}$, where $z = 1, 2, \ldots$ is the iteration number of the SCA method. Accordingly, the left-hand side of (A2) can be approximated as its linear lower bound, and an additional constraint can be obtained as follows:

$$\tau^2 \tilde{v}_n^2 - 2\left(\boldsymbol{p}_n^{U(z)} - \boldsymbol{p}_{n-1}^{U(z)}\right)^T \left(\boldsymbol{p}_n^U - \boldsymbol{p}_{n-1}^U\right) \leq \left\|\boldsymbol{p}_n^{U(z)} - \boldsymbol{p}_{n-1}^{U(z)}\right\|^2, \quad \forall n \in \mathcal{N}. \tag{A3}$$

To handle the nonconvexity of the constraints (22c) and (24), the slack variables $u_{k,n}$ and w_n are introduced for all k, n, which allows us to rewrite (30) as

$$\min_{\{\boldsymbol{p}^U, \boldsymbol{v}, \tilde{\boldsymbol{v}}, \boldsymbol{u}, \boldsymbol{w}\}} \quad \tilde{E}_n^f(v_n, \tilde{v}_n) \tag{A4a}$$

$$\text{s.t.} \quad (1), (24), (20\text{j}), (22\text{c}), (A3) \tag{A4b}$$

$$d_{k,n}^{EU} \leq u_{k,n}, \quad \forall n \in \mathcal{N} \text{ and } \forall k \in \mathcal{K} \tag{A4c}$$

$$d_n^{RU} \leq w_n, \quad \forall n \in \mathcal{N}, \tag{A4d}$$

where we define $\boldsymbol{u} = \{u_{k,n}\}_{\forall k,n}$ and $\boldsymbol{w} = \{w_n\}_{\forall n}$.

In addition, as the $R_{k,n,s}(\boldsymbol{p}_n^U, \boldsymbol{\Theta}_n^I, P_{k,n,s})$ in (24) can be defined as a difference in convex (DC) functions, $R_{k,n,s}$ can be bounded with the slack variables $\boldsymbol{u}$ and $\boldsymbol{w}$ as follows:

$$R_{k,n,s}\left(\boldsymbol{p}_n^U, \boldsymbol{\Theta}_n^I, P_{k,n,s}\right)$$

$$\geq \mathrm{B}\log_2\left(\sum_{\pi_{l.n.j} \geq \pi_{k,n,s}} P_{l,n,j}\left|\tilde{h}_{l,n}\right|^2 + \sigma^2\right) - \mathrm{B}\log_2\left(\sum_{\pi_{l.n.j} > \pi_{k,n,s}} P_{l,n,j}\left|\tilde{h}_{l,n}\right|^2 + \sigma^2\right), \tag{A5}$$

where we have

$$\tilde{h}_{k,n} = \sqrt{\frac{\beta_0}{(u_{k,n})^\zeta} + \frac{\beta_0 M}{w_n (d_k^{ER})^{\epsilon/2}}}, \tag{A6}$$

which is lower-bounded as

$$\begin{aligned}
\left|\tilde{h}_{k,n}\right|^2 &= \left(\frac{A^2}{(u_{k,n})^\zeta} + \frac{B^2}{(w_n)^2} + \frac{2AB}{(u_{k,n})^{\zeta/2} w_n}\right) \\
&\geq M_1^{(z)} - M_2^{(z)}\left(u_{k,n} - u_{k,n}^{(z)}\right) - M_3^{(z)}\left(w_n - w_n^{(z)}\right) \\
&\triangleq \left|\hat{h}_{k,n}\right|^2, \tag{A7}
\end{aligned}$$

with $u_{k,n}^{(z)}$ and $w_n^{(z)}$ being the zth iterate of $u_{k,n}$ and w_n in the SCA algorithm, respectively, $A = \sqrt{\beta_0}$, $B = \frac{\beta_0 M}{(d_k^{ER})^{\epsilon/2}}$,

$$M_1^{(z)} = \left(\frac{A^2}{\left(u_{k,n}^{(z)}\right)^\zeta} + \frac{B^2}{\left(w_n^{(z)}\right)^2} + \frac{2AB}{\left(u_{k,n}^{(z)}\right)^{\zeta/2} w_n^{(z)}}\right), \tag{A8}$$

$$M_2^{(z)} = \left(\frac{\zeta A^2}{\left(u_{k,n}^{(z)}\right)^{\zeta+1}} + \frac{\zeta AB}{\left(u_{k,n}^{(z)}\right)^{\zeta/2+1} w_n^{(z)}}\right) \tag{A9}$$

$$\text{and } M_3^{(z)} = \left(\frac{2B^2}{\left(w_n^{(z)}\right)^3} + \frac{2AB}{\left(u_{k,n}^{(z)}\right)^{\zeta/2}\left(w_n^{(z)}\right)^2}\right). \tag{A10}$$

However, (A5) is neither convex nor concave with respect to $u_{k,n}$ and w_n. To address this issue, we introduce the slack variable $t = \{t_{k,n}\}_{\forall k,n}$ to satisfy $t_{k,n} \leq \left|\hat{h}_{k,n}\right|^2$ and

$$\begin{aligned}
\tilde{R}_{k,n,s}^U &\geq \text{B} \log_2\left(\sum_{\pi_{l.n.j} \geq \pi_{k,n,s}} P_{l,n,j} t_{l,n} + \sigma^2\right) - \text{B} \log_2\left(\sum_{\pi_{l.n.j} > \pi_{k,n,s}} P_{l,n,j} t_{l,n} + \sigma^2\right) \\
&\geq \text{B} \log_2\left(\sum_{\pi_{l.n.j} \geq \pi_{k,n,s}} P_{l,n,j} t_{l,n} + \sigma^2\right) - \text{B} \log_2\left(\sum_{\pi_{l.n.j} > \pi_{k,n,s}} P_{l,n,j} t_{l,n}^{(z)} + \sigma^2\right) \\
&\quad - \frac{\sum_{\pi_{l.n.j} > \pi_{k,n,s}} P_{l,n,j}\left(t_{l,n} - t_{l,n}^{(z)}\right)}{\left(\sum_{\pi_{l.n.j} > \pi_{k,n,s}} P_{l,n,j} t_{l,n}^{(z)} + \sigma^2\right) \log(2)} \\
&\triangleq \hat{R}_{k,n,s}^U. \tag{A11}
\end{aligned}$$

Thus, we can finally have the convex optimization problem (31) for the UAV's trajectory design.

References

1. Mao, Y.; You, C.; Zhang, J.; Huang, K.; Letaief, K.B. A survey on mobile edge computing: The communication perspective. *IEEE Commun. Surv. Tutorials* **2017**, *19*, 2322–2358. [CrossRef]
2. Huang, J.; Wang, M.; Wu, Y.; Chen, Y.; Shen, X. Distributed offloading in overlapping areas of mobile-edge computing for Internet of Things. *IEEE Internet Things J.* **2022**, *9*, 13837–13847. [CrossRef]
3. Yazid, Y.; Ez-Zazi, I.; Guerrero-Gonzalez, A.; El Oualkadi, A.; Arioua, M. UAV-enabled mobile edge-computing for IoT based on AI: A comprehensive review. *Drones* **2021**, *5*, 148. [CrossRef]
4. Bai, T.; Pan, C.; Ren, H.; Deng, Y.; Elkashlan, M.; Nallanathan, A. Resource allocation for intelligent reflecting surface aided wireless powered mobile edge computing in OFDM systems. *IEEE Trans. Wirel. Commun.* **2021**, *20*, 5389–5407. [CrossRef]

5. Wang, F.; Xu, J.; Wang, X.; Cui, S. Joint offloading and computing optimization in wireless powered mobile-edge computing systems. *IEEE Trans. Wirel. Commun.* **2017**, *17*, 1784–1797. [CrossRef]
6. Wang, F.; Zhang, X. IRS/UAV-Based Edge-Computing/Traffic-Offloading Over RF-Powered 6G Mobile Wireless Networks. In Proceedings of the IEEE Wireless Communications and Networking Conference (WCNC), Austin, TX, USA, 10–13 April 2022; pp. 1272–1277.
7. Hu, X.; Wong, K.K.; Zhang, Y. Wireless-powered edge computing with cooperative UAV: Task, time scheduling and trajectory design. *IEEE Trans. Wirel. Commun.* **2020**, *19*, 8083–8098. [CrossRef]
8. Yoo, S.; Jeong, S.; Kang, J. Hybrid UAV-enabled Secure Offloading via Deep Reinforcement Learning. *IEEE Wirel. Commun. Lett.* **2023**, *12*, 972–976. [CrossRef]
9. Jeong, S.; Simeone, O.; Kang, J. Mobile edge computing via a UAV-mounted cloudlet: Optimization of bit allocation and path planning. *IEEE Trans. Veh. Technol.* **2017**, *67*, 2049–2063. [CrossRef]
10. Jeong, S.; Simeone, O.; Kang, J. Mobile cloud computing with a UAV-mounted cloudlet: Optimal bit allocation for communication and computation. *IET Commun.* **2017**, *11*, 969–974. [CrossRef]
11. Liu, Y.; Deng, H.; Peng, C. Channel Estimation for RIS-Assisted MIMO Systems in Millimeter Wave Communications. *Sensors* **2023**, *23*, 5516. [CrossRef]
12. Kumaravelu, V.B.; Imoize, A.L.; Soria, F.R.C.; Velmurugan, P.G.S.; Thiruvengadam, S.J.; Do, D.-T.; Murugadass, A. RIS-Assisted Fixed NOMA: Outage Probability Analysis and Transmit Power Optimization. *Future Internet* **2023**, *15*, 249. [CrossRef]
13. Chapala, V.K.; Zafaruddin, S.M. Multiple RIS-Assisted Mixed FSO-RF Transmission Over Generalized Fading Channels. *IEEE Syst. J.* **2023**, *17*, 3515–3526. [CrossRef]
14. Zhou, F.; Wu, Y.; Hu, R.Q.; Qian, Y. Computation rate maximization in UAV-enabled wireless-powered mobile-edge computing systems. *IEEE J. Sel. Areas Commun.* **2018**, *36*, 1927–1941. [CrossRef]
15. Liu, Y.; Xiong, K.; Ni, Q.; Fan, P.; Letaief, K.B. UAV-assisted wireless powered cooperative mobile edge computing: Joint offloading, CPU control, and trajectory optimization. *IEEE Internet Things J.* **2020**, *7*, 2777–2790. [CrossRef]
16. Zhou, F.;Wu, Y.; Sun, H.; Chu, Z. UAV-enabled mobile edge computing: Offloading optimization and trajectory design. In Proceedings of the IEEE International Conference on Communications (ICC), Kansas City, MO, USA, 20–24 May 201; pp. 1–6.
17. Ghosh, A.; Zhang, J.; Andrews, J.G.; Muhamed, R. *Fundamentals of LTE*; Pearson United Kingdom: London, UK, 2010.
18. Shen, Y.; Dai, W.; Win, M.Z. Power Optimization for Network Localization. *IEEE/ACM Trans. Netw.* **2014**, *22*, 1337–1350. [CrossRef]
19. Hu, X.; Wong, K.K.; Yang, K.; Zheng, Z. UAV-assisted relaying and edge computing: Scheduling and trajectory optimization. *IEEE Trans. Wirel. Commun.* **2019**, *18*, 4738–4752. [CrossRef]
20. Zhou, G.; Pan, C.; Ren, H.; Wang, K.; Nallanathan, A. A Framework of Robust Transmission Design for IRS-aided MISO Communications with Imperfect Cascaded Channels. *IEEE Trans. Signal Process.* **2020**, *68*, 5092–5106. [CrossRef]
21. Wei, Z.; Cai, Y.; Sun, Z.; Ng, D.W.K.; Yuan, J.; Zhou, M.; Sun, L. Sum-rate maximization for IRS-assisted UAV OFDMA communication systems. *IEEE Trans. Wirel. Commun.* **2020**, *20*, 2530–2550. [CrossRef]
22. Li, Z.; Kundu, N.K.; Rao, J.; Shen, S.; McKay, M.R.; Murch, R. Performance analysis of RIS-assisted communications with element grouping and spatial correlation. *IEEE Wirel. Commun. Lett.* **2023**, *12*, 630–634. [CrossRef]
23. Mao, Y.; Dizdar, O.; Clerckx, B.; Schober, R.; Popovski, P.; Poor, H.V. Rate-splitting multiple access: Fundamentals, survey, and future research trends. *IEEE Commun. Surv. Tutorials* **2022**, *24*, 2073–2126. [CrossRef]
24. Katwe, M.; Singh, K.; Clerckx, B.; Li, C.P. Rate Splitting Multiple Access for Sum-Rate Maximization in IRS Aided Uplink Communications. *IEEE Trans. Wirel. Commun.* **2022**, *22*, 2246–2261. [CrossRef]
25. Boyd, S.P.; Vandenberghe, L. *Convex Optimization*; Cambridge University Press: Cambridge, UK, 2004.
26. CVX: Matlab Software for Disciplined Convex Programming. Available online: http://cvxr.com/cvx/ (accessed on 4 September 2023).
27. Wu, Q.; Zhou, X.; Schober, R. IRS-assisted wireless powered NOMA: Do we really need different phase shifts in DL and UL? *IEEE Wirel. Commun. Lett.* **2021**, *10*, 1493–1497. [CrossRef]
28. Zeng, P.; Wu, Q.; Qiao, D. Energy minimization for IRS-aided WPCNs with nonlinear energy harvesting model. *IEEE Wirel. Commun. Lett.* **2021**, *10*, 2592–2596. [CrossRef]
29. Bertsekas, D.P. Nonlinear Programming. *J. Oper. Res. Soc.* **1997**, *48*, 334. [CrossRef]
30. Scutari, G.; Facchinei, F.; Lampariello, L. Parallel and Distributed Methods for Constrained Nonconvex Optimization—Part I: Theory. *IEEE Trans. Signal Process.* **2017**, *65*, 1929–1944. [CrossRef]
31. Zhang, G.; Wu, Q.; Cui, M.; Zhang, R. Securing UAV communications via joint trajectory and power control. *IEEE Trans. Wirel. Commun.* **2019**, *18*, 1376–1389. [CrossRef]